Method for site-specific detection of m6A nucleoside presence in RNA based on high-resolution melting (HRM) analysis

Anna Y. Golovina[1,2,3], Margarita M. Dzama[1,2,3], Kirill S. Petriukov[1,2,3], Timofei S. Zatsepin[1,2,3], Petr V. Sergiev[1,2,3,*], Alexey A. Bogdanov[1,2,3] and Olga A. Dontsova[1,2,3]

[1]Department of Chemistry, Lomonosov Moscow State University, Moscow 119992, Russia, [2]Department of Bioinformatics and Bioengineering, Lomonosov Moscow State University, Moscow 119992, Russia and [3]A.N. Belozersky Institute of Physico-Chemical Biology, Lomonosov Moscow State University, Moscow 119992, Russia

ABSTRACT

Chemical landscape of natural RNA species is decorated with the large number of modified nucleosides. Some of those could easily be detected by reverse transcription, while others permit only high-performance liquid chromatography or mass-spectrometry detection. Presence of m^{6}A nucleoside at a particular position of long RNA molecule is challenging to observe. Here we report an easy and high-throughput method for detection of m^{6}A nucleosides in RNA based on high-resolution melting analysis. The method relies on the previous knowledge of the modified nucleoside position at a particular place of RNA and allows rapid screening for conditions or genes necessary for formation of that modification.

INTRODUCTION

More than a 100 modified nucleoside species could be found in various functional RNA molecules (1). Monitoring of their presence at a particular position of RNA is necessary for the identification of conditions affecting RNA modification as well as for the screening for genes responsible for the modification (2). Some of the modified nucleosides, e.g. m^{2}G and m^{1}A, impede reverse transcription and could easily be detected by primer extension assay (3–6). Others need an additional chemical treatment of modified RNA before reverse transcription. For example, m^{7}G nucleoside serves as a chain breakage point on treatment with NaBH$_4$ followed by incubation with aniline (7,8). Pseudouridine could be revealed by reverse transcription if RNA is pre-treated with N$_2$H$_4$ or

N-cyclohexyl-N′-(2-morpholinoethyl)carbodiimide metho-p-toluenesulfonate and is incubated in a mild basic solution (9). Adenosine nucleosides monomethylated at their exocyclic amino group (m^{6}A) are among the hardest to detect. For monitoring of the m^{6}A presence in a specified RNA position within a large RNA, a short fragment of that RNA should be excised. This could be done with either RNase H cleavage in the presence of the complementary oligodeoxyribonucleotide pair (10) or with unspecific RNase digestion of total RNA, while the selected region is protected by the complementary oligodeoxyribonucleotide (11). After purification of RNA fragment, it should be digested with the specific RNase, usually RNase A or RNase T1. The resulting set of oligoribonucleotides should be analyzed by mass spectrometry. Recently published alternative for this method is an immunoprecipitation with m^{6}A-specific antibodies followed by a massively paralleled sequencing (12,13). Application of this method allowed revealing of thousands of m^{6}A nucleosides in eukaryotic mRNAs. Monitoring of m^{6}A presence at specific RNA positions in a variety of conditions is indispensable for understanding presumable regulatory role of m^{6}A nucleosides.

Here we report a new simple method based on high-resolution melting (HRM) analysis, which allows detection of m^{6}A nucleoside at the specific RNA position. The method could easily be adapted to a high-throughput format.

MATERIALS AND METHODS

Strains and media

Escherichia coli strains BW25113 (WT) (14) and JW5107 (*ΔybiN*), JW1860 (*ΔyecP*), JW4268 (*ΔyjhP*), JW0203

($\Delta yafS$), JW0904 ($\Delta smtA$), JW1123 ($\Delta ymfD$), JW4366 ($\Delta lasT$), JW2565 ($\Delta yfiF$), JW2559 ($\Delta yfiC$), JW3900 ($\Delta yiiV$), JW1859 ($\Delta yecO$), JW5501 ($\Delta ygiQ$), JW0050 ($\Delta ksgA$), JW3466 ($\Delta yhiR$), JW5543 ($\Delta yhdJ$) and JW0200 ($\Delta yafE$) (15) were grown at 37°C in LB media to 0.6 A_{600}. *Bacillus subtilis* transformed with pKH80 plasmid coding for ErmC methyltransferase was grown similarly, with addition of 50 µg/ml ampicillin.

HEK 293 cells (*Homo sapiens*) were cultivated at 37°C, 5.5% CO_2 in Dulbecco's modified Eagle's medium:F12 medium (Invitrogen) supplemented with 10% fetal bovine serum.

Ribosome and RNA preparation

Ribosomes and ribosomal subunits were prepared as described (16). Pure 23 S ribosomal RNA from the strains tested was prepared by phenol extraction out of the 50 S ribosomal subunits (17). Total RNA from bacteria was prepared by QIAGEN RNeasy mini kit. RNA species were stored in deionized water at −80°C. To prepare total tRNA, S100 extract was made by the ultracentrifugation of the cell lysate in MLA-130 rotor (80 000 rpm, 1 h).

S100 was phenol extracted and then small RNA fraction containing all tRNA species was precipitated by 0.3 M NH_4OAc and 80% ethanol solution. Each of RNA isolations was performed three times for three subsequent independent analyses (biological replicas).

Total small RNA fraction (RNAs up to 200-nt long) from 10^8 HEK 293 cells was prepared by Ambion mirVana^{TM} miRNA Isolation Kit. The approximate content of small nuclear RNA (snRNA) U6 was estimated by producing complementary DNA [cDNA; Maxima First Strand cDNA Synthesis Kit for Reverse transcriptase-quantitative polymerase chain reaction (RT-qPCR), Thermo Scientific] and following RT qPCR, while the control during the amplification was U6 coding DNA with known concentration.

Synthetic oligonucleotide probes carrying fluorophore and quencher, and snRNA U6 fragments

We used following pairs of oligonucleotides (B-x–quencher oligodeoxyribonucleotide, F-x–fluorescent oligodeoxyribonucleotide):

Name of oligodeoxy-ribonucleotide	Sequence of oligodeoxyribonucleotide	Complementary region of RNA
Variation of quencher oligodeoxyribonucleotide length (A2030 of 23S rRNA *E.coli*). Figure 1A–D.		
B-2030_1	5′-TCA CAG CG-3′-BHQ1	2023–2030 nt
F-2030_1	FAM-5′-AGT TCA ATT TCA CTG AGT CTC GG-3′	2000–2022 nt
B-2030_2	5′-ATC TTC ACA GCG-3′-BHQ1	2023–2034 nt
F-2030_1	FAM-5′-AGT TCA ATT TCA CTG AGT CTC GG-3′	2000–2022 nt
B-2030_3	5′-CTG CAT CTT CAC AGC G-3′-BHQ1	2023–2038 nt
F-2030_1	FAM-5′-AGT TCA ATT TCA CTG AGT CTC GG-3′	2000–2022 nt
B-2030_4	5′-TACACTGCATCTTCACAGCG-3′-BHQ1	2023–2042 nt
F-2030_1	FAM-5′-AGT TCA ATT TCA CTG AGT CTC GG-3′	2000–2022 nt
Variation of fluorescent oligodeoxyribonucleotide length (A2030 of 23S rRNA *E.coli*). Figure 1E–H.		
B-2030_3	5′-CTG CAT CTT CAC AGC G-3′-BHQ1	2023–2038 nt
F-2030_5	FAM-5′-AGT TCA ATT TCA CTG AGT-3′	2005–2022 nt
B-2030_3	5′-CTG CAT CTT CAC AGC G-3′-BHQ1	2023–2038 nt
F-2030_6	FAM-5′-AGT TCA ATT TCA CTG AGT CT-3′	2003–2022 nt
B-2030_3	5′-CTG CAT CTT CAC AGC G-3′-BHQ1	2023–2038 nt
F-2030_1	FAM-5′-AGT TCA ATT TCA CTG AGT CTC GG-3′	2000–2022 nt
B-2030_3	5′-CTG CAT CTT CAC AGC G-3′-BHQ1	2023–2038 nt
F-2030_7	FAM-5′-AGT TCA ATT TCA CTG AGT CTC GGG T-3′	1998–2022 nt
Analysis of m⁶A methylation in A2030 of 23S rRNA *E.coli*. Figure 2A, 3–6.		
B-2030_8	5′-TAC ACT GCA TCT T-3′-BHQ1	2030–2042 nt
F-2030_8	FAM-5′-CAC AGC GAG TTC AAT TTC ACT GA-3′	2007–2029 nt
Analysis of m⁶A methylation in A2030 of 23S rRNA *E.coli*. Figure 2B–D		
B-2030_9	5′-GTA CAC TGC ATC TTC A-3′-BHQ1	2028–2043 nt
F-2030_9	FAM-5′-CAG CGA GTT CAA TTT CAC TGA GT-3′	2005–2027 nt
B–2030_2	5′-ATC TTC ACA GCG-3′-BHQ1	2023–2034 nt
F-2030_1	FAM-5′-AGT TCA ATT TCA CTG AGT CTC GG-3′	2000–2022 nt
B-2030_10	5′-CATCTTCACAGCGAGTTCAA-3′-BHQ1	2016–2035 nt
F-2030_10	FAM-5′-TTT CAC TGA GTC TCG GGT GGA GA-3′	1993–2015 nt
Analysis of m⁶A methylation in A37 of tRNA$^{Val}_1$ *E.coli*. Figure 7A–C		
B-37_1	5′-GAC CCC CTC CTT-3′-BHQ1	37–48 nt
F-37_1	FAM-5′-GTA AGG GAG GTG CTC TCC CAG CT-3′	14–36 nt
B-37_2	5′-CCC CCT CCT TGT A-3′-BHQ1	34–46 nt
F-37_2	FAM-5′-AGG GAG GTG CTC TCC CAG CTG AG-3′	11–33 nt
B-37_3	5′-CTT GTA AGG-3′-BHQ1	32–39 nt
F-37_3	FAM-5′-GAG GTG CTC TCC CAG CTG AGC TA-3′	8–31 nt
Analysis of m⁶A methylation in A1618 of 23S rRNA *E.coli*. Figure 7D		
B-1618	5′-GAC CAC CTG TGT-3′-BHQ1	1614–1625 nt
F-1618	FAM-5′-CG GTT TGG GGT ACG ATT TGA TGT-3′	1591–1613 nt
Analysis of m⁶A methylation in A2085 of 23S rRNA *B.subtilis*. Figure 7E		
B-2085	5′-CGG GGT CTT TCC GT-3′-BHQ1	2081–2094 nt

(continued)

Continued

Name of oligodeoxy-ribonucleotide	Sequence of oligodeoxyribonucleotide	Complementary region of RNA
F-2085	FAM-5′-CCT GTC GCG GGT AAC CTG CAT CT-3′	2058–2080 nt
Analysis of m6A methylation in A43 of snRNA U6 *H.sapiens*. Figure 7F		
F-U6	FAM-5′-GTATCGTTCCAATTTTAGTATATGTGCTGC-3′	13–54 nt
B-U6	5′-CTAATCTTCTCTG-3′-BHQ1	
Fragments of U6 snRNA *H.sapiens* with and without m6A used for method calibration		
U6 + m6A	5′-GCUUCGGCAGCACAUAUACUAAAAUUGGAACGAUAC <u>**m6dA**</u>GAGAAGAUUAGCAUGGCCCCUG-3′	7–65 nt
U6-m6A	5′-<u>GCU</u>UCGGCAGCACAUAUACUAAAAUUGGAACGAUAC <u>**dA**</u>GAGAAGAUUAGCAUGGCCCCUG-3′	7–65 nt

Probes hybridization and HRM analysis

Each hybridization and melting experiment was reproduced in three technical and three biological replicas (total nine replicas minimum). If not indicated otherwise, for hybridization and melting experiment, 0.4 µM of individual RNA or RNA mixture was combined with 0.4-µM BHQ-x oligonucleotide and 0.2-µM FAM-x oligonucleotide in optically clear PCR tubes. Ionic conditions for the hybridization were 50 mM Tris-HCl, pH 8.3, and 40 mM KCl, the volume of mixture was 10 µl. The mixture was placed into the qPCR analyzer; in our case, we used CFX96 Real-Time System (Bio-Rad). The hybridization was done by heating to 80°C for 3 min followed by cooling to 20°C at a rate 3°/min. Melting curve were obtained by steady heating back to 80°C at a rate 1°/min in increments of 0.5° and monitoring of FAM fluorescence. Fluorescence curves were normalized and differential curves were analyzed. The standard representations of differential fluorescence curves produced by HRM analysis software (18) were shown.

To measure the suitability of melting analysis at various RNA concentrations, essentially the same protocol was used, whereas the concentrations of the 23S rRNA and oligonucleotides were taken as indicated in the text and figures. The total 23S rRNA concentration was kept constant at 0.4 µM, whereas the composition varied from 100% of methylated 23S rRNA purified from the wild-type strain to 100% of unmethylated 23S rRNA purified from the JW3466 (*ΔyhiR*) strain (11) in increments of 10%. For detection of tRNA$^{Val}_1$ modification at m6A37, 4 µg of total tRNA was taken for each probe. For detection of m6A presence in *H. sapiens* U6 snRNA, 1.4 µg of total small RNA fraction from HEK 293 cells was taken for each probe, which corresponds to 1.4 pmol (0.14 µM) of U6 snRNA according to RT qPCR quantification. Same amount of pure synthetic analog of U6 snRNA fragment either containing m6dA43 or unmethylated dA43 was used as a control. We used m6dA instead of m6A because of lack of any commercially available m6A precursor for chemical synthesis of RNA.

RESULTS

Modified nucleosides in DNA and RNA could influence base-pairing or base-stacking interactions, which could alter melting properties of nucleic acid duplexes (19). We explored the possibility to use melting properties of RNA–DNA duplex to monitor presence of modified nucleosides. We used the segment of *E. coli* 23S rRNA with the modified nucleoside m6A2030 as a first model. According to our previously published data, this nucleoside is completely modified in the wild-type *E. coli* strain, while being completely unmodified in the JW3466 (*ΔyhiR*) strain, lacking the A2030-specific rRNA methyltransferase (11). To test the utility of HRM analysis for the monitoring of adenosine modification, we designed a set of oligodeoxyribonucleotide pairs complementary to the RNA target (Figures 1 and 2). One oligonucleotide in each pair was modified with 6-carboxyfluorescein (FAM) fluorophore at its 5′-end, whereas the other one carried Black Hole Quencher (BHQ1) quencher at its 3′-end. Sequences of both probes are designed in such a way that they should hybridize to target RNA side-by-side, bringing fluorophore and quencher to immediate juxtaposition (Figures 1 and 2). Modified RNA nucleoside is always located within the borders of area covered with the shorter quencher-containing oligonucleotide.

We tested how melting curves of BHQ1-containing oligonucleotides are affected by A2030 nucleoside modification. These BHQ1-containing oligonucleotides share the same 3′-end region and have variable length of 8, 12, 16 and 20 nt. All of them are shorter than FAM-containing oligonucleotide, whose length was 23 nt (Figure 1). We assumed that fluorescence of FAM would be affected by the melting of the shorter BHQ1-containing oligonucleotides, and this melting would be dependent on the presence of the modification in RNA. Obtained differential melting curves demonstrated dependence on the A2030 modification (Figure 1B and C) in such a way that the modification lowered Tm of the shorter oligonucleotide. The recommendation regarding the length of BHQ1-containing oligonucleotide is that it should be sufficiently large to effectively hybridize to the RNA, unlike 8mer oligonucleotide (Figure 1A), but it has to be as small as possible to get the maximal difference in Tm for the modified and unmodified RNA (see decrease in ΔTm in Figure 1B to C to D).

The length of the FAM-containing oligonucleotide was changed in the next set of the experiments (Figure 1E–H). We tested the 18-, 20-, 23- and 25-nt long FAM-
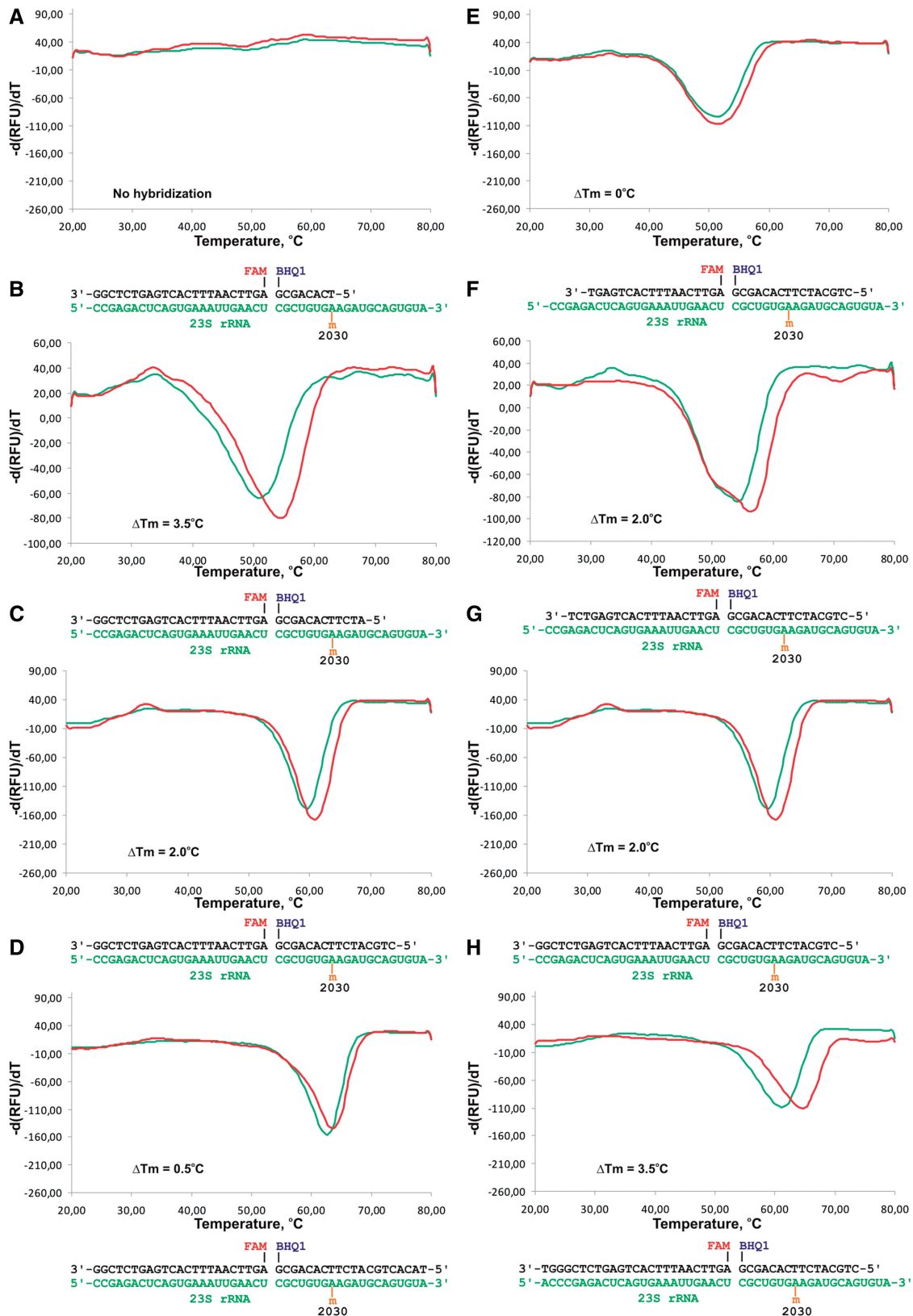
Figure 1. Optimization of probe length. Differential melting curves of duplexes formed by the 23S rRNA from the wild-type and Δ*yhiR* knockout strains of *E. coli* and a set of pairs of oligonucleotide probes. Schemes of oligonucleotide probes hybridization to the target-modified RNA molecule are depicted below each panel. Green curves correspond to the wild-type strain (23S rRNA modified at m⁶A2030), and red curves correspond to Δ*yhiR* knockout strain (23S rRNA unmodified at A2030). The length of probes varied as follows: (**A**) FAM probe 23 nt, BHQ1 probe 8 nt; (**B**) FAM probe 23 nt, BHQ1 probe 12 nt; (**C**) FAM probe 23 nt, BHQ1 probe 16 nt; (**D**) FAM probe 23 nt, BHQ1 probe 20 nt; (**E**) FAM probe 18 nt, BHQ1 probe 16 nt; (**F**) FAM probe 20 nt, BHQ1 probe 16 nt; (**G**) FAM probe 23 nt, BHQ1 probe 16 nt; and (**H**) FAM probe 25 nt, BHQ1 probe 16 nt.
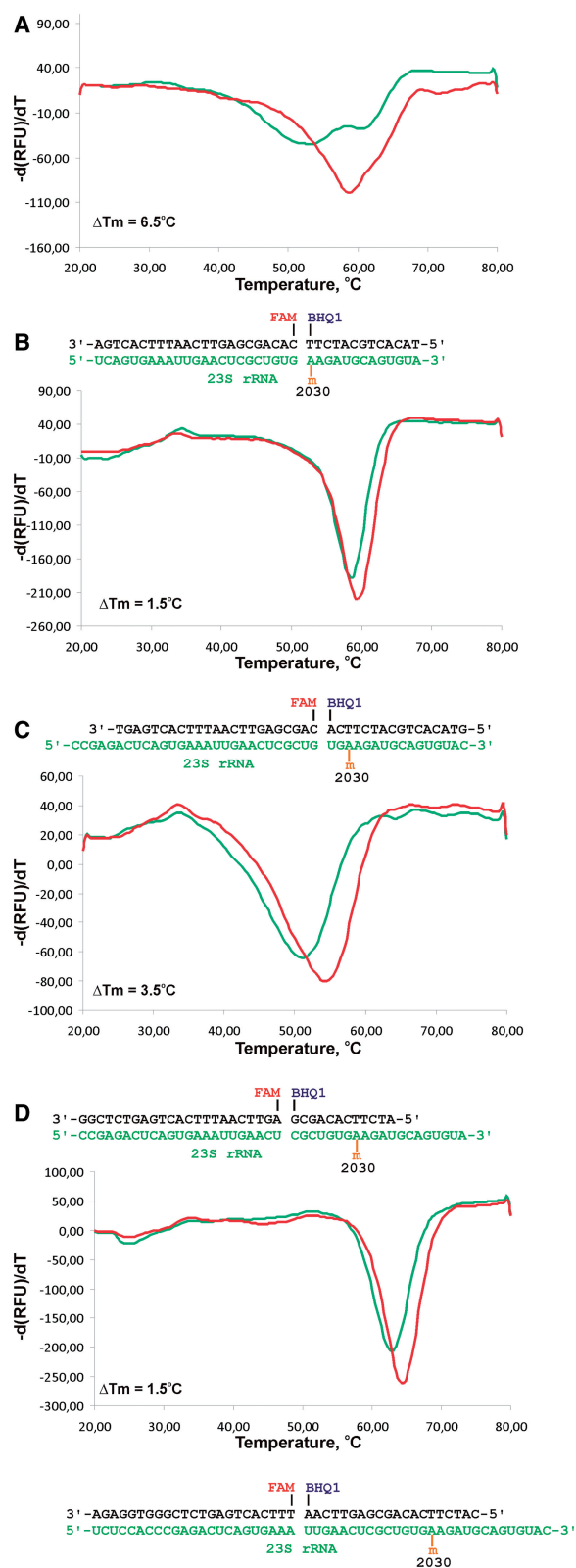
Figure 2. Optimization of probe location relative to modified nucleoside. Differential melting curves of duplexes formed by the 23S rRNA from the wild-type and Δ*yhiR* knockout strains of *E. coli* and a set of pairs of oligonucleotide probes. Schemes of oligonucleotide probes hybridization to the target-modified RNA molecule are depicted below each panel. Green curves correspond to the wild-type strain (23S rRNA modified at m6A2030), and red curves correspond to Δ*yhiR* knockout

containing oligonucleotides combined with the single 16-nt long BHQ1-containing oligonucleotide. The shortest FAM-containing oligonucleotide demonstrated no dependence of Tm on the RNA modification (Figure 1E). We assume that similar differential curves in this case result from the early melting of the duplex formed by the RNA and FAM-containing oligonucleotide, before the melting of the BHQ1-containing oligonucleotide duplex, which is hybridized with the modification site of RNA. The longer is the FAM-containing oligonucleotide (see Figure 1E to F to G to H), the greater is the difference in melting curves for modified and unmodified RNAs.

To optimize hybridization position of BHQ1-containing oligonucleotide relative to the site of the modification in RNA, we tested four pairs of BHQ1 and FAM-containing oligonucleotides (Figure 2). BHQ1-containing oligonucleotides hybridized to different areas of RNA so that the modification site is either complementary to the 3′-end of the quencher oligonucleotide (Figure 2A), or to the middle part of the quencher oligonucleotide (Figure 2B and C) or to the 5′-end region of the quencher oligonucleotide (Figure 2D). We observed much more effect of the BHQ1-oligonucleotide length rather than of the position of quencher oligonucleotide relative to the modified nucleoside in RNA. Curiously, the pair of oligonucleotides hybridized in such a way that modification site in RNA, located opposite to the site of BHQ1 attachment, produced the most pronounced difference between melting curves for modified and unmodified RNAs (Figure 2A). Duplexes formed by oligonucleotide probes with the 23S rRNA carrying methylated nucleoside A2030 melts via biphasic process with two melting peaks at 43°C and 52°C, whereas the duplex formed by the unmethylated 23S rRNA melts at 49°C (Figure 2A). Maximal difference between the methylated and unmethylated RNAs is manifested at 49°C. This pair of oligonucleotides (B-2030_8 and F-2030_8) was chosen for several further experiments.

Could the observation of melting curves of RNA with selected oligonucleotide pair be helpful in searching for gene responsible for particular RNA modification via screening a set of bacterial strains carrying gene knockouts? To answer this question, we chose a set of strains each of which lacked particular gene coding for actual or hypothetical RNA methyltransferase, namely, Δ*ybiN*, Δ*yecP*, Δ*yjhP*, Δ*yafS*, Δ*smtA*, Δ*ymfD*, Δ*lasT*, Δ*yfiF*, Δ*yfiC*, Δ*yiiV*, Δ*yecO*, Δ*ygiQ*, Δ*ksgA*, Δ*yhiR*, Δ*yhdJ* and Δ*yafE* strains (15). The wild-type strain (14) was used as a control. The 23S rRNA was extracted from these strains and was studied by HRM analysis for the m6A2030 presence (Figure 3). In all the strains, except Δ*yhiR* strain (11), nucleoside A2030 is modified. Accordingly, we can see highly similar differential melting curves of the 23S rRNA–oligonucleotide duplexes for rRNA from

Figure 2. Continued
strain (23S rRNA unmodified at A2030). The length of probes varied as follows: (**A**) m6A nucleoside hybridize opposite to the 3′-end of BHQ1 probe; (**B**) m6A nucleoside hybridize at a 3-nt distance from the 3′-end of BHQ1 probe; (**C**) m6A nucleoside hybridize at a 8-nt distance from the 3′-end of BHQ1 probe; (**D**) m6A nucleoside hybridize at a 15-nt distance from the 3′-end of BHQ1 probe.
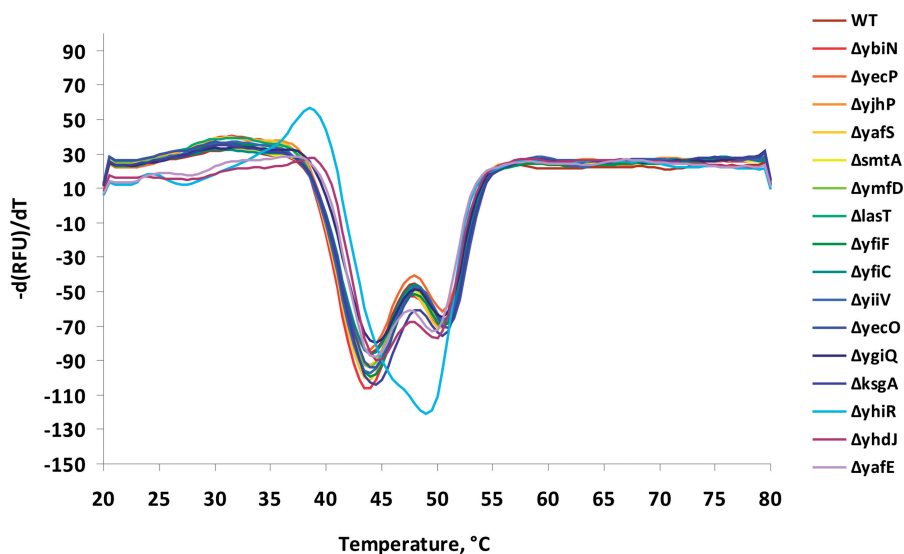
Figure 3. Applicability of the method for screening a set of knockout strains in a search for specific RNA methyltransferase gene. Differential melting curves of duplexes formed by a pair of oligonucleotide probes, shown in Figure 2A, and the 23S rRNA from the wild-type and the set of *E. coli* knockout strains. Key to the figure is shown on the right.

all of these strains, including wild-type rRNA. Only the duplex formed by the oligonucleotides and the 23S rRNA from the strain *ΔyhiR*, which lacks A2030 modification, displayed clearly altered melting properties (Figure 3).

We checked if we could detect m⁶A in modified RNA being mixed with unmodified RNA of the same sequence. To this end, we prepared a set of mixtures of the 23S rRNA containing m⁶A2030 from the wild-type strain with that from *ΔyhiR* strain, devoid of the modification at A2030. We used a set of mixtures of modified and unmodified RNA in different proportions ranging from 100% of modified RNA to 100% of unmodified in increments of 10%. The total concentration of RNA was 0.4 μM. The resulting HRM curves of the mixtures changed steadily from the 100% of methylated RNA to 100% of unmethylated, displaying roughly an additive contribution of respective pure RNA species (Figure 4). Approximately 30% of admixture of RNA containing m⁶A2030 with unmodified one can be detected.

Our next goal was to determine the minimal amount of the RNA, whose modification we could detect using HRM-based method. To do so, we tested the melting behavior of 23S rRNA:B-2030_8:F-2030_8 complexes with the concentration ratios of: 1 μM:1 μM:0.5 μM, 0.4 μM:0.4 μM:0.2 μM, 0.2 μM:0.2 μM:0.1 μM, 0.1 μM: 0.1 μM:0.05 μM and 0.05 μM:0.1 μM:0.025 μM. 0.02 μM: 0.02 μM:0.01 μM (Figure 5). The amplitude of the fluorescence change decreased with the decrease of RNA concentration. The concentrations of 0.1 μM of 23S rRNA, 0.1 μM B-2030_8 oligonucleotide and 0.05 μM F-2030_8 oligonucleotide were found to be minimal for the decisive identification of the RNA modification. In 10-μl volume, the quantity of RNA equals to 1 pmol, that corresponds to the amount of rRNA extracted from $5 \cdot 10^4$ bacterial cells. The molar ratio of 0.4 μM:0.4 μM: 0.2 μM seems to be optimal for clear implementing of the method.

Hybridization of oligonucleotide probes to RNA is specific and thus the presence of bulk cellular RNA should not interfere with the detection of the modification at the specific site in the particular RNA. We compared the melting curve analysis done with the purified RNA from the large ribosomal subunit (Figure 6A) with that of total cellular RNA (Figure 6B). Use of total RNA proved to be as effective as usage of purified RNA in melting curve assay for the detection of the m⁶A2030 modification.

To test the universality of the method, we used four additional models having the modified nucleoside in the different primary and secondary structure contexts. First is the *E. coli* tRNA$^{Val}_1$ that contains nucleoside m⁶A37 modified by methyltransferase YfiC. We designed three pairs of oligonucleotides complementary to tRNA$^{Val}_1$ (Figure 7A–C) and investigated melting of their duplexes with total small RNA fraction from the wild-type and *ΔyfiC* strains (Figure 7A–C). Application of the quencher-containing B-37_1 oligonucleotide that hybridizes with the region 37–48 nt of tRNA$^{Val}_1$ produced highly different melting curves for the RNA prepared from the wild-type and *ΔyfiC* strain. A distinct melting peak was observed for only unmodified tRNA$^{Val}_1$, whereas no melting was evident for the modified RNA sample (Figure 7A). This difference could be explained by overall lack of oligonucleotide hybridization to the modified tRNA$^{Val}_1$. Modified nucleosides in tRNA are known to stabilize its structure (20) and it is likely that such stabilization prevents efficient competition of complementary oligonucleotide with the secondary and tertiary structure of tRNA. Shifting oligonucleotide hybridization position by two nucleotides (Figure 7B) has not changed the principal difference between the curves corresponding to the modified and unmodified tRNAs. However, for both samples, a peak at similar higher temperature could be observed (Figure 7B, 72°C), which could represent either melting of a duplex formed by
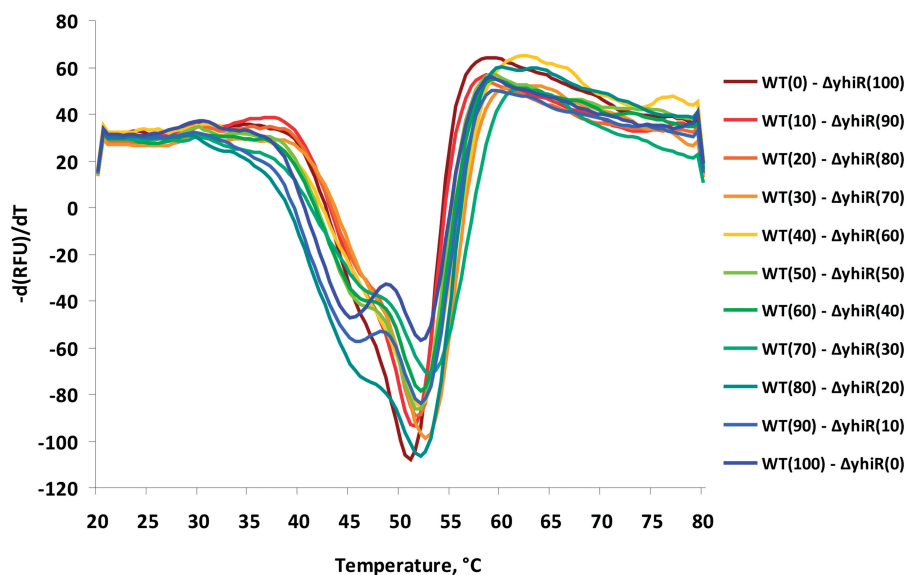
Figure 4. Differential melting curves of duplexes formed by the mixtures of the 23S rRNA from the wild-type *E. coli* strain and Δ*yhiR* knockout strain and a pair of oligonucleotide probes, shown on the Figure 2A. The percentage of RNA from each strain is indicated on the right of the figure.

FAM-containing oligonucleotide or other structural rearrangement independent of the modification. Further movement of hybridization position resulted in complete loss of hybridization with both the modified and unmodified tRNA (Figure 7C). Lack of hybridization could be explained by the smaller length of the BHQ-containing oligonucleotide. Alternatively, the presence of other modified nucleoside, uridine 5-oxyacetic acid, in the middle of the tRNA region complementary to the oligonucleotide prevents its hybridization.

As a second additional model, we used the *E. coli* 23S rRNA carrying m^6A modification at a nucleoside 1618, which is formed by YbiN methyltransferase. The pair of B-1618 and F-1618 oligonucleotides allowed to observe a reproducible difference between curves for the methylated 23S rRNA from the wild-type and for the unmethylated 23S rRNA from Δ*ybiN* strain (Figure 7D). The difference observed for the m^6A1618 modification resembled that for m^6A2030 modification (Figure 1). In both cases, modification resulted in lower melting temperature of the RNA–DNA hybrid.

We make use of 23S rRNA adenosine 2058 (*E. coli* numbering) dimethylation introduced by ErmC methyltransferase, an enzyme that causes macrolide resistance in a number of bacteria (21) as our third additional model. Ribosomal RNA was purified from *B. subtilis* transformed with the plasmid coding for ermC gene. The similar RNA sample from untransformed *B. subtilis* was used as a control. We used pair of oligonucleotides B-2085 and F-2085 complementary to *B. subtilis* 23S rRNA (Figure 7E). The area of B-2085 oligonucleotide complementarity in the 23S rRNA contained modified m^6_2A2085, the nucleoside corresponding to *E. coli* m^6_2A2058. Because adenosine dimethylation completely abolish Watson-Crick base pairing, we observed drastic difference between the melting curves corresponding to the modified and unmodified 23S rRNA (Figure 7E). Melting curve corresponding to unmodified 23S rRNA contain a single pronounced peak, while the melting behavior of the duplex formed by modified 23S rRNA demonstrated several shallow peaks.

Finally, we demonstrated that the method is suitable for the detection of m^6A presence in eukaryotic non-ribosomal RNA. To this end, we used one of the few m^6A residues in human RNA, which was previously identified at a single-nucleotide resolution, namely, m^6A43 of U6 snRNA (22). Unfortunately, an enzyme responsible for this modification is unknown. Thus, we first compared model chemically synthesized fragments of U6 snRNA containing m^6dA43 or dA43. We used deoxynucleosides due to the unavailability of the m^6A ribonucleotide precursor for the RNA chemical synthesis. After initial optimization of the fluorescent and quencher oligonucleotide length, we chose the most optimal pair (Figure 7F). In complete agreement with our results on the previous models, we observed decrease in the melting temperature on m^6A modification (Figure 7F, red curve–unmodified versus green curve–modified). Because the enzyme responsible for m^6A43 formation in U6 snRNA is unknown, we compared a melting curve corresponding to the natural U6 snRNA present in a total small RNA fraction of human HEK 293 cells with that of control chemically synthesized U6 snRNA fragments. In agreement with our expectations, a melting curve corresponding to the natural human U6 snRNA (Figure 7F, blue curve) demonstrated even lower Tm than the methylated control RNA. The difference between the curves corresponding for the m^6dA-containing model RNA and the natural U6 snRNA could be attributed to other modifications present in natural U6 snRNA, such as several 2'OMe and Ψ.

DISCUSSION

Hereby we report a method for monitoring the presence of m^6A nucleoside in a specific position of long RNA
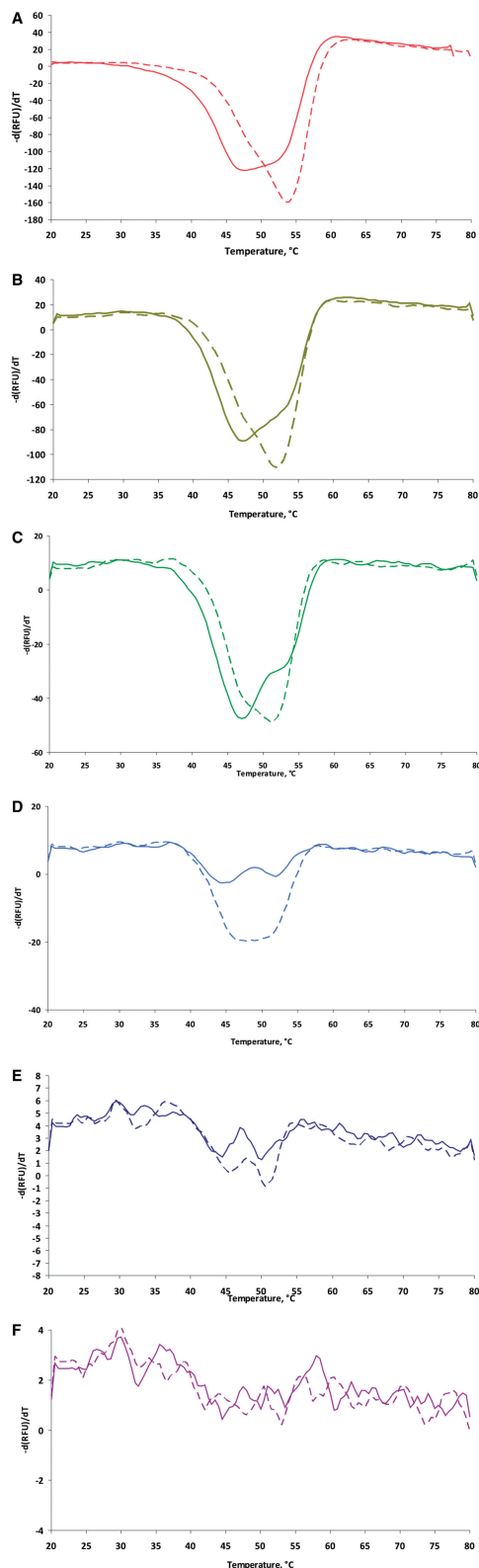
Figure 5. Sensitivity of the method. Differential melting curves of duplexes formed by the 23S rRNA from the wild-type *E. coli* strain (solid curves) and *ΔyhiR* knockout strain (dashed curves) and a pair of oligonucleotide probes, shown in Figure 2A at different concentrations of the tested RNA and probes. The 23S rRNA:BHQ1-probe:FAM-probe ratios are as follows: $1\,\mu M{:}1\,\mu M{:}0.5\,\mu M$ (**A**), $0.4\,\mu M{:}0.4\,\mu M{:}0.2\,\mu M$ (**B**), $0.2\,\mu M{:}0.2\,\mu M{:}0.1\,\mu M$ (**C**), $0.1\,\mu M{:}0.1\,\mu M{:}0.05\,\mu M$ (**D**), $0.05\,\mu M{:}0.1\,\mu M{:}0.025\,\mu M$ (**E**) and $0.02\,\mu M{:}0.02\,\mu M{:}0.01\,\mu M$ (**F**).

molecule using HRM analysis. Adenosine nucleosides methylated at their exocyclic amino group are hard to detect (3). Primer extension analysis could not be used for this purpose because m^6A does not affect reverse transcription of RNA. RNA fragment excision and cleavage followed by mass-spectrometry is extremely laborious and could not be scaled up to high-throughput analysis. RNA immunoprecipitation via anti-m^6A antibody followed by massively parallel sequencing allows transcriptome-wide identification of m^6A nucleosides with 50–100 nt fidelity (12,13). However, it could be hardly used to screen many samples in a high-throughput assay. The method described here allows easy screening for the m^6A presence at a particular position of RNA using total RNA sample and qPCR machine. Although the monomethylation of adenosine exocyclic amino group does not lead to alteration in hydrogen bonding within the nucleic acid duplex, it affects stacking interactions and accordingly its melting properties (19).

Highly precise monitoring of fluorescence in the course of duplex melting is widely used for the monitoring polymorphisms in DNA (23). It was also reported to be useful for studying RNA editing (24) and DNA methylation (25). Both methods described in the literature rely on the changes in nucleic acid sequence and as such are extensions of basic mutation detection technique based on HRM. Here we demonstrated the suitability of HRM method for the direct monitoring of the modified nucleoside presence in the RNA molecules. In contrast to the previously published methods it does not rely on the change in nucleic acid sequence and does not involve any PCR-based amplification. The method described here relies directly on the alteration of nucleic acids duplex melting properties resulting from the RNA modification.

According to our data, the presence of m^6A in the RNA part of the RNA–DNA duplex lowers its melting temperature. The extent of Tm shift increases with the decrease in length of the quencher-containing oligonucleotide; however, the short quencher-containing oligonucleotide could fail to hybridize with RNA especially if the RNA target possesses strong secondary structure. We recommend 12–13-nt-long probes containing a quencher and >20-nt long probes, containing a fluorophore. We also could advise to design a quencher-containing oligonucleotide in such a way that after hybridization with RNA, the modified RNA nucleoside would be directly opposite to the 3′-terminal nucleotide carrying the quencher.

We demonstrated the universality of the method. The detection of m^6A nucleosides at three specific positions of rRNA, one position of tRNA and one position of snRNA was successful. Not only purified-specific RNA, but also a bulk cellular RNA is suitable for detection of m^6A at a pre-defined position due to the specificity of oligonucleotide probe hybridization. Non-ribosomal targets need partial enrichment, such as simple molecular weight-based purification, easily accomplished by commercially available kits.

Possible application of the method is the screening of the knockout/knockdown strain libraries in a search for the gene responsible for the formation of particular m^6A nucleoside. Another possible application is the detection
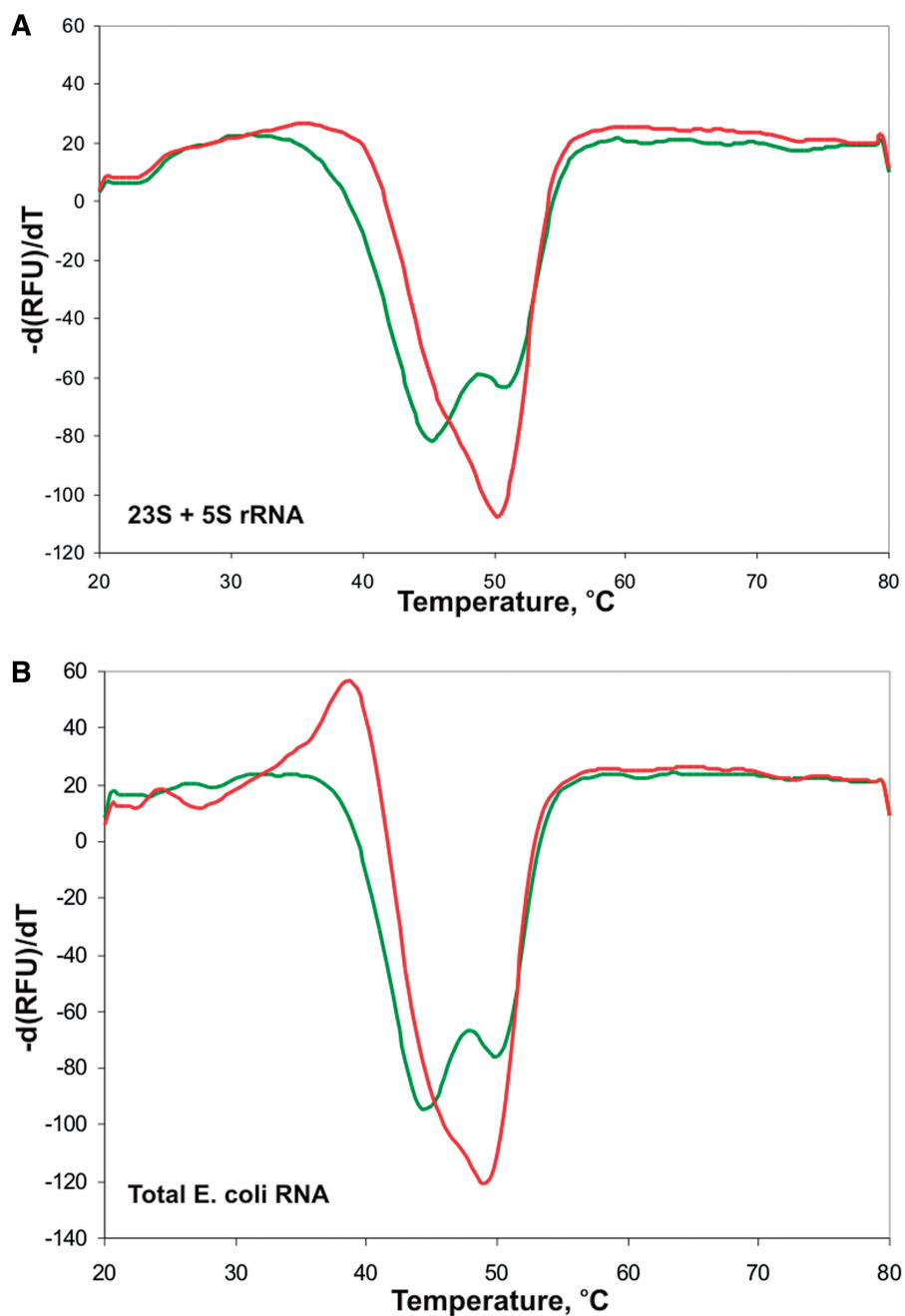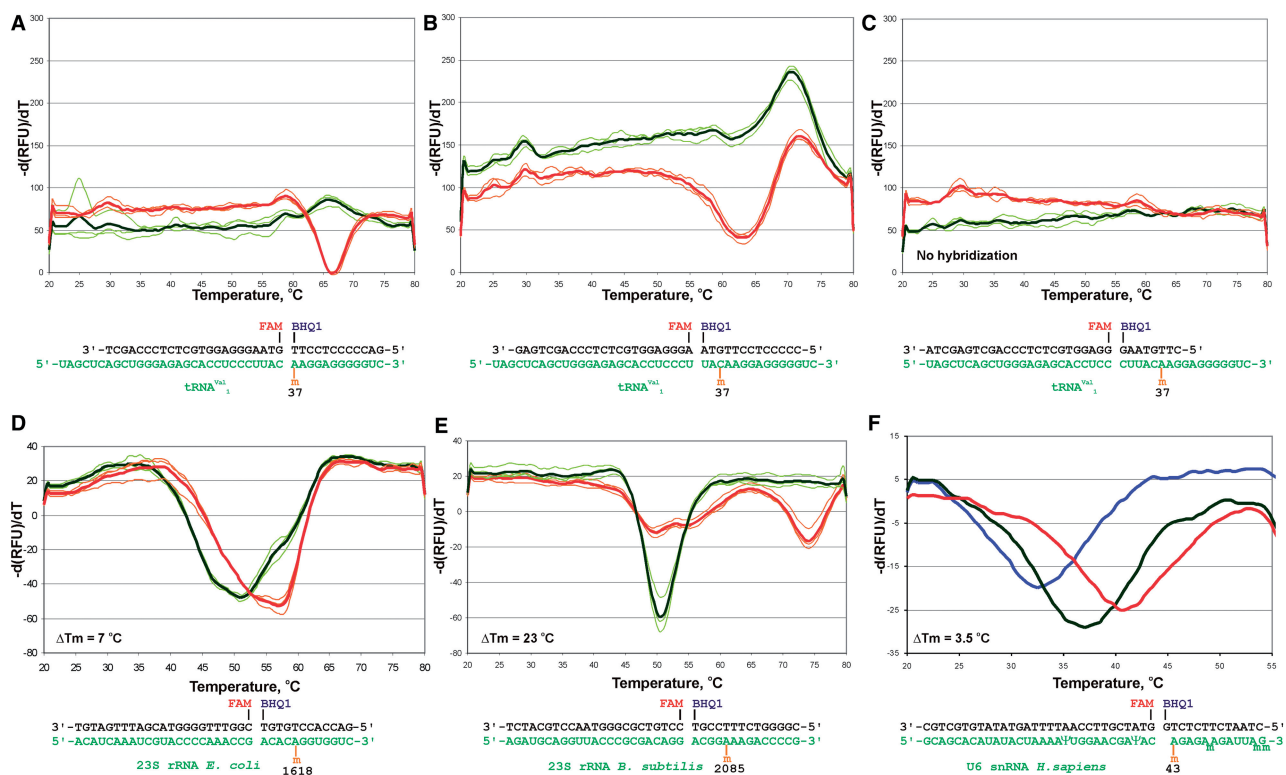
Figure 6. Applicability of the method for bulk cellular RNA. Differential melting curves of duplexes formed by the RNA samples from the wild-type and ΔyhiR knockout strains of *E. coli* and a pair of oligonucleotide probes shown in Figure 2A. Green curves correspond to the wild-type strain (23S rRNA modified at m^{6}A2030), and red curves correspond to ΔyhiR knockout strain (23S rRNA unmodified at A2030). (**A**) Purifieid rRNA from the large ribosomal subunit was used for hybridization with probes; (**B**) Bulk cellular RNA was used for hybridization with probes.

of the particular m^{6}A nucleoside presence at various growth or environmental conditions. The overwhelming majority of modified nucleosides in eukaryotic and particularly human mRNAs are m^{6}A nucleosides (12,13). Given particular types of mRNA are present at the quantity of up to 10 000 per mammalian cell (26), 10^7 cells would be required to analyze methylation of abundant mRNA with the help of HRM method. However, it is advisable to apply partial mRNA enrichment, such as affinity purification via polyA tails. The role

of these modified nucleosides still remains mysterious, while some important regulatory role is likely. The proposed method might help to decipher dynamic events which lead to modification of particular RNAs. Before the application of the described method to eukaryotic mRNA, positions of the modified residues have to be mapped with the nucleotide resolution. We demonstrated the suitability of the method to study eukaryotic RNA species exemplified by U6 snRNA. The latter is the rare example of eukaryotic RNAs where precise position of

Figure 7. Applicability of the method for other m^6A nucleosides in RNA. (**A–C**) Differential melting curves of duplexes formed by the $tRNA^{Val}_1$ from the wild-type and $\Delta yfiC$ knockout strains of *E. coli* and a set of pairs of oligonucleotide probes. Schemes of oligonucleotide probes hybridization to the target-modified RNA molecule are depicted below each panel. Green curves correspond to the wild-type strain (tRNA modified at m^6A37), and red curves correspond to $\Delta yfiC$ knockout strain (tRNA unmodified at A37). (**D**) Differential melting curves of duplexes formed by the 23S rRNA samples from the wild-type strain of *E. coli* and $\Delta ybiN$ knockout strain. Scheme of oligonucleotide probes hybridization to the target-modified RNA molecule is depicted below the panel. Green curves correspond to the wild-type strain (23S rRNA modified at m^6A1618), and red curves correspond to $\Delta ybiN$ knockout strain (23S rRNA unmodified at A1618). (**E**) Differential melting curves of duplexes formed by the 23S rRNA samples from either untransformed *B. subtilis* or *B. subtilis* transformed with plasmid pKH80 encoding ErmC methyltransferase. Scheme of oligonucleotide probes hybridization to the target-modified RNA molecule is depicted below the panel. Green curves correspond to the untransformed strain (23S rRNA unmodified at A2085), and red curves correspond to the strain transformed by pKH80 (23S rRNA modified at m^6_2A2085). (**F**) Differential melting curves of duplexes formed by the synthetic fragments of U6 snRNA containing either m^6dA43 (green curve) or $dA43$ (red curve). Melting curve corresponding to natural human U6 snRNA purified from HEK 293 cell line is colored blue. Scheme of oligonucleotide probe hybridization to the target-modified RNA molecule is depicted below the panel.

m^6A has been mapped. Because an enzyme responsible for m^6A formation in U6 snRNA is unknown, the designed system that could be used for the screening of putative methyltransferase knockout or knockdown cell lines in a search for such an enzyme.

Another application of this method could be the monitoring of modified nucleosides in rRNA that cause antibiotic resistance. A number of m^6A methyltransferases mono- or dimethylate the nucleoside A2058 of the 23S rRNA [for reviews see (27,28)]. This modification leads to the resistance to macrolide antibiotics (21). The method described in this work was tested for monitoring such modifications as well. Presence of other modified nucleosides whose presence in the RNA would cause alteration in melting could also be monitored by the method described.

ACKNOWLEDGEMENTS

FUNDING

REFERENCES

1. Machnicka,M.A., Milanowska,K., Osman Oglou,O., Purta,E., Kurkowska,M., Olchowik,A., Januszewski,W., Kalinowski,S., Dunin-Horkawicz,S., Rother,K.M. *et al.* (2013) MODOMICS: a database of RNA modification pathways—2012 update. *Nucleic Acids Res.*, **41**, D262–D267.
2. Sergiev,P.V., Golovina,A.Y., Prokhorova,I.V., Sergeeva,O.V., Osterman,I.A., Nesterchuk,M.V., Burakovsky,D.E., Bogdanov,A.A. and Dontsova,O.A. (2011) Modifications of ribosomal RNA: from enzymes to function. In: Rodnina,M.V.,

Wintermeyer,W. and Green,R. (eds), *Ribosomes*. Springer, Vienna, pp. 97–110.

3. Sergiev,P.V., Osterman,I.A., Prokhorova,I.V., Nesterchuk,M.V., Sergeeva,O.V., Golovina,A.I., Demina,I.A., Galiamina,M.A., Serebriakova,M.V. and Dontsova,O.A. (2011) Systems biology approach to the functional role of enzymatic modification of bacterial ribosome [in Russian]. *Bioorg. Khim.*, **37**, 81–90.

4. Lesnyak,D.V., Osipiuk,J., Skarina,T., Sergiev,P.V., Bogdanov,A.A., Edwards,A., Savchenko,A., Joachimiak,A. and Dontsova,O.A. (2007) Methyltransferase that modifies guanine 966 of the 16 S rRNA: functional identification and tertiary structure. *J. Biol. Chem.*, **282**, 5880–5887.

5. Lesnyak,D.V., Sergiev,P.V., Bogdanov,A.A. and Dontsova,O.A. (2006) Identification of *Escherichia coli* m2G methyltransferases: I. the ycbY gene encodes a methyltransferase specific for G2445 of the 23 S rRNA. *J. Mol. Biol.*, **364**, 20–25.

6. Sergiev,P.V., Lesnyak,D.V., Bogdanov,A.A. and Dontsova,O.A. (2006) Identification of *Escherichia coli* m2G methyltransferases: II. The ygjO gene encodes a methyltransferase specific for G1835 of the 23 S rRNA. *J. Mol. Biol.*, **364**, 26–31.

7. Wintermeyer,W. and Zachau,H.G. (1975) Tertiary structure interactions of 7-methylguanosine in yeast tRNA Phe as studied by borohydride reduction. *FEBS Lett.*, **58**, 306–309.

8. Zueva,V.S., Mankin,A.S., Bogdanov,A.A. and Baratova,L.A. (1985) Specific fragmentation of tRNA and rRNA at a 7-methylguanine residue in the presence of methylated carrier RNA. *Eur. J. Biochem.*, **146**, 679–687.

9. Bakin,A.V. and Ofengand,J. (1998) Mapping of pseudouridine residues in RNA to nucleotide resolution. *Methods Mol. Biol.*, **77**, 297–309.

10. Sergiev,P.V., Serebryakova,M.V., Bogdanov,A.A. and Dontsova,O.A. (2008) The ybiN gene of *Escherichia coli* encodes adenine-N6 methyltransferase specific for modification of A1618 of 23 S ribosomal RNA, a methylated residue located close to the ribosomal exit tunnel. *J. Mol. Biol.*, **375**, 291–300.

11. Golovina,A.Y., Dzama,M.M., Osterman,I.A., Sergiev,P.V., Serebryakova,M.V., Bogdanov,A.A. and Dontsova,O.A. (2012) The last rRNA methyltransferase of *E. coli* revealed: the yhiR gene encodes adenine-N6 methyltransferase specific for modification of A2030 of 23S ribosomal RNA. *RNA*, **18**, 1725–1734.

12. Dominissini,D., Moshitch-Moshkovitz,S., Schwartz,S., Salmon-Divon,M., Ungar,L., Osenberg,S., Cesarkas,K., Jacob-Hirsch,J., Amariglio,N., Kupiec,M. *et al.* (2012) Topology of the human and mouse m6A RNA methylomes revealed by m6A-seq. *Nature*, **485**, 201–206.

13. Meyer,K.D., Saletore,Y., Zumbo,P., Elemento,O., Mason,C.E. and Jaffrey,S.R. (2012) Comprehensive analysis of mRNA methylation reveals enrichment in 3′ UTRs and near stop codons. *Cell*, **149**, 1635–1646.

14. Datsenko,K.A. and Wanner,B.L. (2000) One-step inactivation of chromosomal genes in *Escherichia coli* K-12 using PCR products. *Proc. Natl Acad. Sci. USA*, **97**, 6640–6645.

15. Baba,T. and Mori,H. (2008) The construction of systematic in-frame, single-gene knockout mutant collection in *Escherichia coli* K-12. *Methods Mol. Biol.*, **416**, 171–181.

16. Blaha,G., Stelzl,U., Spahn,C.M., Agrawal,R.K., Frank,J. and Nierhaus,K.H. (2000) Preparation of functional ribosomal complexes and effect of buffer conditions on tRNA positions observed by cryoelectron microscopy. *Methods Enzymol.*, **317**, 292–309.

17. Knud H. Nierhaus (1990) Reconstitution of ribosomes. *Ribosomes and Protein Synthesis: A Practical Approach*. IRL press, Oxford, pp. 161–188.

18. Precision Melt Analysis™ Software | Life Science Research | Bio-Rad.

19. Kierzek,E. and Kierzek,R. (2003) The thermodynamic stability of RNA duplexes and hairpins containing N6-alkyladenosines and 2-methylthio-N6-alkyladenosines. *Nucleic Acids Res.*, **31**, 4472–4480.

20. Motorin,Y. and Helm,M. (2010) tRNA Stabilization by modified nucleotides. *Biochemistry*, **49**, 4934–4944.

21. Skinner,R., Cundliffe,E. and Schmidt,F.J. (1983) Site of action of a ribosomal RNA methylase responsible for resistance to erythromycin and other antibiotics. *J. Biol. Chem.*, **258**, 12702–12706.

22. Shimba,S., Bokar,J.A., Rottman,F. and Reddy,R. (1995) Accurate and efficient N-6-adenosine methylation in spliceosomal U6 small nuclear RNA by HeLa cell extract *in vitro*. *Nucleic Acids Res.*, **23**, 2421–2426.

23. Vossen,R.H.A.M., Aten,E., Roos,A. and den Dunnen,J.T. (2009) High-resolution melting analysis (HRMA): more than just sequence variant screening. *Hum. Mutat.*, **30**, 860–866.

24. Chateigner-Boutin,A.-L. and Small,I. (2007) A rapid high-throughput method for the detection and quantification of RNA editing based on high-resolution melting of amplicons. *Nucleic Acids Res.*, **35**, e114.

25. Wojdacz,T.K. and Dobrovic,A. (2007) Methylation-sensitive high resolution melting (MS-HRM): a new approach for sensitive and high-throughput assessment of methylation. *Nucleic Acids Res.*, **35**, e41.

26. Alberts,B., Bray,D., Lewis,J., Raff,M., Roberts,K. and Watson,J.D. (1994) *Molecular Biology of the Cell 3E*, 3rd edn. Garland Science, New York.

27. Weisblum,B. (1995) Erythromycin resistance by ribosome modification. *Antimicrob. Agents Chemother.*, **39**, 577–585.

28. Mankin,A.S. (2008) Macrolide myths. *Curr. Opin. Microbiol.*, **11**, 414–421.